This article has been accepted for publication in a future issue of this journal, but has not been fully edited. Content may change prior to final publication. Citation information: DOI 10.1109/TPEL.2017.2768244, IEEE Transactions on Power Electronics

Multi-MHz IPT Systems for Variable Coupling

Juan M. Arteaga, Samer Aldhaher, George Kkelis, David C. Yates, and Paul D. Mitcheson,
Department of Electrical and Electronic Engineering
Imperial College London
j.arteaga-saenz15@imperial.ac.uk

***Abstract*—In typical Multi-MHz Inductive Power Transfer (IPT) systems, a change in coupling or load resistance can significantly deteriorate the end-to-end efficiency due to a deviation from the optimal load of the IPT-link and sub-optimal operation of the resonant inverter due to the loss of soft switching condition. This paper proposes solutions for an IPT system to operate efficiently when large changes in coupling take place. To achieve high power-efficiency independent of coupling, we utilise inherent regulation properties of resonant converters to avoid losing soft switching for any coupling value, and present the optimal load to the IPT-link at the maximum energy-throughput coupling. A probability-based model is introduced to assess and optimise the IPT system by analysing coupling as a distribution in time, which depends on the dynamic behaviour of the wireless charging system. The proposed circuits are a Class D rectifier with a resistance compression network (RCN) in the receiving-end and a load-independent Class EF inverter in the transmitting-end. Experiments were performed at 6.78 and 13.56 MHz verifying high efficiency for dynamic coupling and variable load resistance. End-to-end efficiencies of up to 88% are achieved at a coil separation larger than one coil-radius for a system capable of supplying 150 W to the load, and the energy-efficiency was measured at 80% when performing a uniformly-distributed linear-misalignment of 0-12.5 cm, corresponding to a receiver moving at constant velocity over a transmitter without power throughput control.**

I. Introduction

ONE of the essential advantages of utilising wireless power transfer (WPT) systems is the possibility of mobility for the device being charged. This feature is crucial in highly dynamic low-power applications such as powering biomedical implants, and in higher power applications such as dynamic charging of electric vehicles (EV). In this paper we consider the dynamic charging of devices using multi-MHz frequencies at power levels typically lower than $1\,\mathrm{kW}$.

An IPT system consists of three main power conversion blocks: the coil driver which is a high frequency inverter, the IPT-link which exchanges power between two loosely-coupled inductors (often referred as IPT-coils), and the rectifier at the receiving-end. Additional power conversion blocks can be integrated to the system at both ends, however the analysis of this paper considers the end-to-end power conversion as dc-input power to dc-output power as shown in Fig. 1.

The end-to-end efficiency of an IPT system can be calculated as:

$$\begin{aligned}\eta_{\mathrm{dc-dc}} &= \eta_{\mathrm{inv}}\eta_{\mathrm{link}}\eta_{\mathrm{rect}} \\ &= \eta_{\mathrm{t}}\eta_{\mathrm{r}},\end{aligned} \tag{1}$$

where η_{inv} and η_{rect} are the efficiencies of the coil-driver and the rectifier respectively, the transmitting-end efficiency (η_{t}) accounts for the losses in the coil driver and the transmitting-coil, and the receiving-end efficiency (η_{r}) considers the losses in the receiving coil and the rectifier circuit.

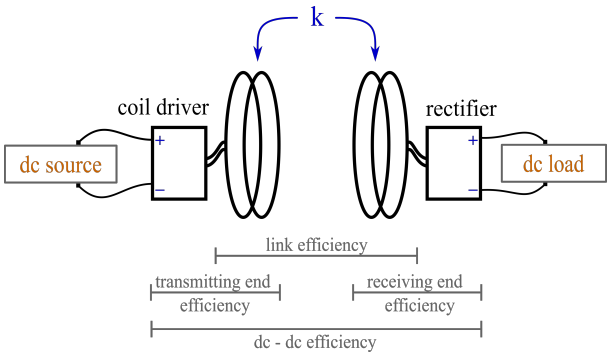


Fig. 1. Diagram of an IPT system.

The end-to-end efficiency of an IPT system depends partially on the type of application and the specific design being utilised. For example, existing designs in high-power IPT systems allow end-to-end efficiencies of more than $90\,\%$ [1]–[3] to be achieved. These designs are usually proposed for the application identified in [1] as one of the biggest challenges for IPT: wireless EV charging. IPT for EV charging has henceforth encouraged the concept of not only transferring power while the receiving-end is stationary, but also transferring power while the device being charged is moving. Unlike our work presented here, typical high power IPT systems for dynamic charging operate at frequencies lower than $100\,\mathrm{kHz}$, where the IPT-coils are designed to shape the magnetic flux of the IPT-link with magnetically permeable materials in order to maintain a consistently high coupling factor throughout the range of motion of the system [4], [5]. An alternative approach to reduce the variation of coupling against uni-dimensional movement was shown in [6] for lower power ($150\,\mathrm{W}$) $6.78\,\mathrm{MHz}$ IPT systems using multiple-transmitter air-core coils, which adds complexity.

In contrast, this paper describes the design of a dynamic air-cored two-coil IPT system operating at multi-MHz frequencies. The main incentive to operate IPT systems at multi-MHz frequencies, usually at the ISM bands of 6.78, 13.56 and $27.12\,\mathrm{MHz}$, is that at these frequencies IPT systems do not tend to require magnetic cores to shape and enhance the magnetic flux of the IPT-link. This can be beneficial, not only because the losses in the magnetic cores are eliminated, but most notably because air-core coils tend to be significantly

This work is licensed under a Creative Commons Attribution 3.0 License. For more information, see http://creativecommons.org/licenses/by/3.0/.

This article has been accepted for publication in a future issue of this journal, but has not been fully edited. Content may change prior to final publication. Citation information: DOI 10.1109/TPEL.2017.2768244, IEEE Transactions on Power Electronics

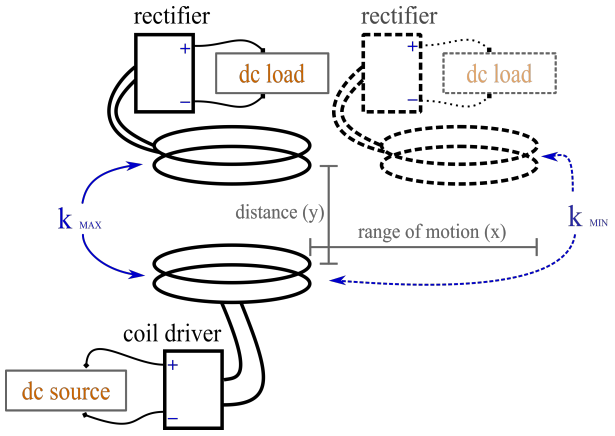


Fig. 2. Dynamic wireless charger diagram.

lighter than ferrite-core coils, which is an alternative feature in many portable applications. For example in [7], an off-the-shelf drone without a battery was wirelessly powered in mid-air with a 13.56 MHz IPT system, where the receiving-end coil consisted of solely a single turn of copper conductor surrounding the propellers guard structure of the drone. The design of an IPT system to power a device capable of moving freely has to account for the coupling variation throughout the range of motion of the system regardless of its specific architecture. The effects of variable coupling for multi-MHz IPT systems, as represented in Fig. 2, tend to be large considering that IPT systems using air-core coils have a limited capability of shaping the magnetic flux of the link, and therefore spatial freedom implies a significant variance in coupling.

As in high-power low-frequency IPT systems, high efficiency can be achieved in multi-MHz IPT systems [8]–[12], because at these frequencies the quality factor (Q-factor) of the coils is sufficiently high to compensate for low coupling. The range of power of IPT systems that use air-core coils tends to be limited to a few hundred watts; nonetheless, good efficiencies have been reported in multi-MHz inverters and rectifiers at high power [13], [14] and the design of a 3.3 kW vehicle charging system using air-core coils and operating at 3 MHz has been proposed [15].

The circuits at both ends of multi-MHz IPT systems are usually based on Class E or Class D resonant topologies given their soft-switching capabilities, which are necessary to achieve high efficiency at such frequencies. Typical resonant topologies, however, tend to be very susceptible to load variations and when these are implemented in IPT systems the susceptibility to load variations translates to a susceptibility to changes in the receiver electrical load as well as the geometry of the link. In [8], a Class E inverter was utilised as the coil driver in a 150 W multi-MHz IPT system for the first time. That work shows the system operating at various coil misalignments, however the system frequency had to be tuned for different couplings, to avoid suboptimal operation of the inverter. Optimal operation is necessary to avoid excessive heating and not affect the integrity of the transistor at these power levels. Lower power IPT systems using a Class E inverter, such as the one presented in [16] (P_o <20 W) can be designed to tolerate changes in coupling even with suboptimal operation of the inverter (i.e with a load resistance different than the optimal one) at different couplings and still achieve reasonably good end-to-end efficiencies for high values of coupling (14-44 %) due to the performance of the available components at these power levels.

This paper first provides an overview of IPT theory considering the effect of variable coupling. There are two variables that can compensate for variations in coupling to therefore achieve constant power throughput or constant output voltage without detuning the system: the input voltage of the inverter and the dc-load. Accounting for changes in coupling and these two variables motivated the selection and design of the proposed topologies at both ends of the IPT system aiming to account for minimum impact on the end-to-end efficiency. A load-independent Class EF inverter, introduced in [17], is proposed as the coil-driver since it inherently achieves ZVS for the entire load range, and unlike a typical Class E inverter provides an output current magnitude that is independent of the load resistance and directly proportional to the input voltage of the inverter. Therefore, the output current can be easily adjusted or controlled. The latter feature of this inverter is analysed in this work for the first time. The proposed rectifier is based on a RCN Class D configuration that allows the input resistance of the rectifier to be designed to the value that achieves the maximum link-efficiency at highest system energy-throughput. This combination of resonant converters was introduced in our work [11].

The dynamic charging environment of an IPT system is then modelled using probability theory to account for typical characteristics of dynamic charging such as mobile autonomy of the device being charged. The proposed model is useful to identify a value of coupling factor to design the circuits at both ends of the system and achieve the highest energy-efficiency throughout the charging time. This model, introduced in this paper, is a general expression that applies and can be useful to optimise, for maximum energy-efficiency, any IPT system in which coupling is variable. Additionally, this model can be used to assess an IPT system against changes in coupling, and therefore help bound what could be considered an acceptable range of coupling.

The design of a 150 W IPT system for dynamic charging is then presented and corroborated by sets of experiments at 6.78 and 13.56 MHz, where the inherent properties of the resonant converters are verified by the consistently high end-to-end efficiency achieved for a broad range of coupling factor: 4 to 10.5 % for the system at 6.78 MHz and 2 to 4.9 % for the system at 13.56 MHz. The peak efficiency in both experiments (88 % at 6.78 MHz and 83 % at 13.56 MHz) is, to the authors' knowledge, the highest dc-dc efficiency ever achieved with the corresponding coil separations at such frequencies. These experiments also show, for the first time, an IPT system with a power capability of 150 W operating at variable coupling lower than 12 % at 6.78 MHz and lower than 5 % at 13.56 MHz.

The theoretical analysis and equations presented in this paper are for series-tuned-secondary IPT systems because the proposed topology of the rectifier is current-driven; however,

This work is licensed under a Creative Commons Attribution 3.0 License. For more information, see http://creativecommons.org/licenses/by/3.0/.

This article has been accepted for publication in a future issue of this journal, but has not been fully edited. Content may change prior to final publication. Citation information: DOI 10.1109/TPEL.2017.2768244, IEEE Transactions on Power Electronics

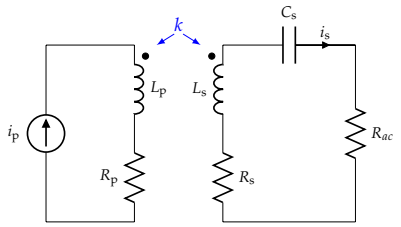


Fig. 3. Equivalent circuit model of an IPT system with a series-tuned secondary.

the same design principle for variable coupling can be applied to the equations for parallel-tuned-secondary IPT systems described in [18].

II. Variable Coupling in Loosely-Coupled IPT Systems

Dynamic wireless charging environments exhibit a variable coupling factor (k), as the relative position of the receiving-end of an IPT system changes with respect to the transmitting-end. The value of k can be calculated in terms of the self-inductance of the transmitting-coil (L_p), the receiving coil (L_s) and the mutual inductance (M_ps), which changes as the relative position of the coils changes:

$$k = \frac{M_\mathrm{ps}}{\sqrt{L_\mathrm{p} L_\mathrm{s}}}. \tag{2}$$

This dimensionless variable, along with the Q-factor of the coils, can be used to describe the exchange of energy between coupled inductors and account for the losses in an inductive link.

A. Link-Efficiency for Variable Coupling

The losses in an inductive link, which in many cases represent a dominant part of the total losses of the system, are represented in Fig. 3 as the power dissipated in the equivalent-series-resistance (ESR) of the coils, R_p and R_s respectively. These losses can be calculated using the expression of the link-efficiency given by [18] for a series-resonant secondary IPT system:

$$\eta_\mathrm{link} = \frac{k^2 Q_\mathrm{p} \alpha}{\left(\alpha + k^2 Q_\mathrm{p} + \frac{1}{Q_\mathrm{s}}\right)\left(\alpha + \frac{1}{Q_\mathrm{s}}\right)}, \tag{3}$$

where:

$$\alpha = \omega_\mathrm{res} C_\mathrm{s} R_\mathrm{ac},$$

Q_p and Q_s are the Q-factors of the transmitting and receiving-coils, defined as:

$$Q_\mathrm{p} = \frac{\omega_\mathrm{res} L_\mathrm{p}}{R_\mathrm{p}}, Q_\mathrm{s} = \frac{\omega_\mathrm{res} L_\mathrm{s}}{R_\mathrm{s}}, \tag{4}$$

where ω_res is the resonant angular operating frequency, C_s is the capacitance of the receiving-end resonant tank, and R_ac is an ac-load, which in systems with a dc-output, represents the real component of the input impedance of the rectifier at the frequency of operation.

The highest link-efficiency for given Q_p, Q_s, and k is achieved when the rectifier has an input resistance equal to the optimal load ($R_{\mathrm{ac}_\mathrm{opt}}$), which can be calculated by solving

$$\frac{\partial \eta_\mathrm{link}}{\partial R_\mathrm{ac}} = 0$$

for R_ac:

$$R_{\mathrm{ac}_\mathrm{opt}} = \frac{1}{\omega_\mathrm{res} C_\mathrm{s}} \left(\frac{\sqrt{1 + k^2 Q_\mathrm{p} Q_\mathrm{s}}}{Q_\mathrm{s}} \right). \tag{5}$$

When the relative position of the coils changes from maximum coupling to a lower coupling, it not only causes the link-efficiency to drop, but also causes $R_{\mathrm{ac}_\mathrm{opt}}$ to change. This implies that as the coils change their relative position, R_ac should change accordingly to achieve the highest link efficiency for any given k.

Notwithstanding the fact that decreasing the coupling factor has negative impact on the link-efficiency, it can be minimised by selecting coils and frequencies of operation that achieve higher unloaded Q-factors. When the Q-factor of the coils is increased, the link-efficiency becomes less dependent of the value of k and in the deviation of R_ac from $R_{\mathrm{ac}_\mathrm{opt}}$. This allows achieving a high link-efficiency for a broader range of k and R_ac.

B. Power Regulation for Variable Coupling

Several variables can be managed to compensate for the changes in k in order to achieve constant receiver output voltage or power. Fig. 3 shows a circuit that represents an IPT-link with a series-tuned secondary. In this circuit, R_ac and the root-mean-square (RMS) of the current in the transmitting-coil ($i_{\mathrm{p}_\mathrm{rms}}$) are set as candidate variables to control the power output without affecting resonance in the receiving-end.

The dc-output power of an IPT system (P_o), also expressed as the squared dc output voltage (V_o^2) divided by the dc load resistance (R_dc), can be calculated by referring the load resistance to the primary, as follows:

$$P_\mathrm{o} = \frac{{V_\mathrm{o}}^2}{R_\mathrm{dc}} = {i_{\mathrm{p}_\mathrm{rms}}}^2 R_\mathrm{eq} \eta_\mathrm{r}, \tag{6}$$

where R_eq, which is the reflected resistance of the receiving-end to the transmitting-end, is dependent on the actual load on the receiver and the coupling factor:

$$R_\mathrm{eq} = \frac{k^2 L_\mathrm{p}}{C_\mathrm{s}\left(R_\mathrm{ac} + R_\mathrm{s}\right)}. \tag{7}$$

Both (6) and (7) are valid only when the secondary circuit is tuned at the frequency of i_p, which for a series-tuned secondary circuit is:

$$f_{i_\mathrm{p}} = \frac{1}{2\pi\sqrt{L_\mathrm{s} C_\mathrm{s}}}. \tag{8}$$

In order to keep either V_o or P_o constant, the variables R_ac and $i_{\mathrm{p}_\mathrm{rms}}$ can be controlled to compensate for changes in coupling factor without detuning the receiving-end circuit. The drawbacks, however, of using the resistance of the dc-load, and consequently R_ac, to control the amount of transferred power is that the link-efficiency deteriorates when deviating

This work is licensed under a Creative Commons Attribution 3.0 License. For more information, see http://creativecommons.org/licenses/by/3.0/.

This article has been accepted for publication in a future issue of this journal, but has not been fully edited. Content may change prior to final publication. Citation information: DOI 10.1109/TPEL.2017.2768244, IEEE Transactions on Power Electronics

$R_{\rm ac}$ from its optimal value. Therefore, using $R_{\rm ac}$ as a control variable should be avoided unless the end-to-end efficiency is not a top priority (e.g. [19]) or when the link-efficiency is high enough so that the variance of $R_{\rm ac}$, within the control range, has no significant impact on end-to-end efficiency of the system. Controlling the amplitude of the current in the transmitting-coil is a suitable alternative to regulate the output power and maintain the highest link-efficiency, in which case a communication-link between the transmitting-end and the receiving-end is necessary to deliver the correct amount of power required by the load.

III. Inherent Regulation in Resonant Converters for Variable Coupling

In multi-MHz IPT systems, the coil-driver and the rectifier are most commonly designed using resonant power converter topologies in order to reduce the switching losses of the semiconductor devices.

Regulating the output voltage or the output current in resonant converters is more challenging than in those based on hard-switching pulse width modulation (PWM), because the soft-switching condition depends not only on the passive component values, but also on the duty cycle and usually the load resistance. Therefore, if the duty cycle or the load are changed once the circuit is tuned, the converter typically loses its soft-switching operation which severely affects the efficiency of the circuit. There are designs where it is possible to control the converter output voltage or current and maintain soft-switching, such as the phase-controlled full-bridge Class D dc-dc converter, which has an output voltage that depends on the phase difference between the signals driving each of the branches of the inverting stage. Another technique that can potentially help dynamically tune or control the power throughput in resonant converters was proposed in [20], where a saturable reactor was integrated in a Class E inverter to compensate for changes in the load. On-off or hysteresis control can also be used to perform voltage or current regulation in resonant converters as can a regular PI loop with PWM.

The inherent regulation properties of resonant converters can sometimes be used to maintain soft switching, for instance, non-synchronous Class E rectifiers inherently change the duty cycle of the diode when the dc-load changes, and consequently achieve ZVS. Furthermore, in [21] a hybrid Class E rectifier (a Class E rectifier with an additional capacitance that provides an additional degree of design freedom) not only achieves ZVS, but also can be designed to inherently regulate the output voltage as the load changes. The inherent regulation properties of resonant converters have been utilised for multiple purposes, for example in [22] the resonant nature of a LCC converter was utilised for power factor correction, and in [23] an inherent over-current protection feature was implemented by placing an auxiliary circuit in parallel with the resonant capacitor of a LLC resonant converter which shorts the capacitor and detunes the resonant tank when a fault shorts out the load.

The proposed multi-MHz converters at both ends of the dynamic IPT system in our work described here do not require a closed loop control system to achieve optimum operation. They exploit the inherent regulation properties of resonant converters to not be affected when changes in the geometry of the IPT-coils and the dc-load are presented.

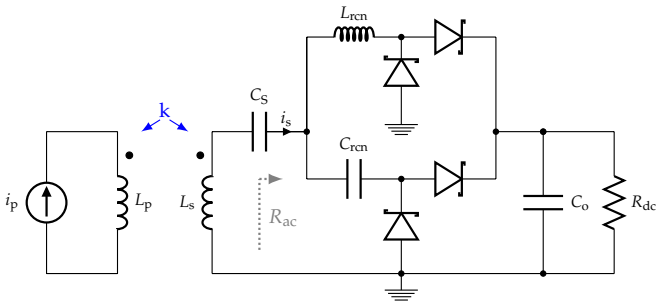


Fig. 4. Class D rectifier with a RCN in an IPT system.

A. RCN-Class D Rectifier for Variable Coupling

Resistance compression networks were introduced in [24], [25] to inherently regulate the input resistance of a rectifier with changes in the dc-load. This principle has also been implemented in RF transmission lines for long-range WPT systems [26], and in IPT [27].

The concept is based on feeding a dc-load with two separate rectifiers, each with an additional reactive impedance connected either in series or in parallel, depending if the rectifier is current-driven or voltage-driven. These two supplemental reactive impedances should be designed to be complex-conjugates at the frequency of operation so that the equivalent impedance seen by the source is real (i.e. resistive). This creates a compressed dependency between the input resistance of the circuit and the dc-load resistance. The input resistance also depends on the magnitude of the reactance ($X_{\rm rcn}$) of the supplemental reactive impedances,

$$X_{\rm rcn} = 2\pi f_{\rm ip} L_{\rm rcn} = \frac{1}{2\pi f_{\rm ip} C_{\rm rcn}}, \tag{9}$$

which allows the circuit to be designed with a range of input impedances to optimally load the magnetic link. Hence, $X_{\rm rcn}$ can be treated as an independent design variable.

This concept can be further extrapolated to a higher order RCNs to achieve better compression, as proposed for transmission-line RCN in [26], where four rectifiers were connected to the source via two stages of reactive impedances. This approach, nonetheless, is difficult to implement in multi-MHz IPT because the parasitics of the printed circuit board (PCB) and the tolerance in the off-the-shelf passive components, would make these very difficult to tune.

The proposed topology, seen in Fig. 4, uses a first order RCN and two current-driven Class D rectifiers. The magnitude of the reactance of $C_{\rm rcn}$ and $L_{\rm rcn}$ is equal at the frequency of operation, therefore the circuit can be modelled as a resistance ($R_{\rm ac}$), and the design of the series-tuned secondary of the IPT system can be performed accordingly.

The input resistance of the rectifier shown in Fig. 4 is:

$$R_{ac} = \frac{L_{\rm rcn}}{2R_{\rm rect}C_{\rm rcn}}\left(1 + \frac{C_{\rm rcn}R_{\rm rect}^2}{L_{\rm rcn}}\right), \tag{10}$$

This work is licensed under a Creative Commons Attribution 3.0 License. For more information, see http://creativecommons.org/licenses/by/3.0/.

This article has been accepted for publication in a future issue of this journal, but has not been fully edited. Content may change prior to final publication. Citation information: DOI 10.1109/TPEL.2017.2768244, IEEE Transactions on Power Electronics

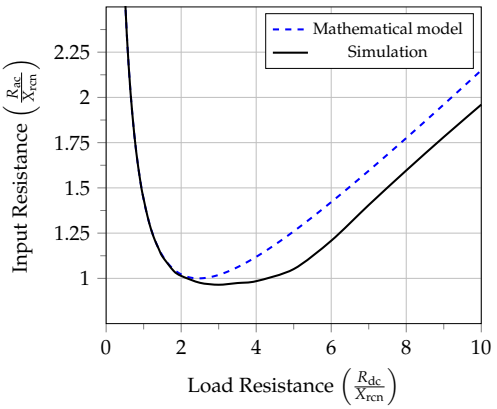


Fig. 5. Input resistance of the RCN-Class D rectifier.

where $R_{\rm rect}$ represents the input resistance of each Class D rectifier. In [28], the input resistance of a current-driven Class D rectifier is calculated as:

$$R_{\text{class D}} = \frac{2R_{\rm L}}{\pi^2 \eta_{\rm rect}}, \tag{11}$$

and since the dc-load ($R_{\rm dc}$) is powered by both branches of the rectifier, $R_{\rm L}$ in (11) corresponds to $2R_{\rm dc}$, and therefore:

$$R_{\rm rect} = \frac{4R_{\rm dc}}{\pi^2 \eta_{\rm rect}}. \tag{12}$$

Modelling the input resistance of this rectifier as shown in (10), has its limitations when the value of $R_{\rm rect}$ is greater than $X_{\rm rcn}$, since the Class D rectifiers enter a discontinuous mode of operation. This happens because the sinusoidal current waveform at the input of the Class D rectifiers deteriorates as $R_{\rm rect}$ increases against a fixed value of $X_{\rm rcn}$.

Fig. 5 shows how $R_{\rm ac}$ changes with $R_{\rm dc}$, from both the mathematical model proposed in [25] and a SPICE simulation considering ideal components and an ideal sinusoidal current source at the input of the circuit. The plots in Fig. 5 show that the input resistance of the proposed topology has a compressed dependence on the dc-load and that it can be designed by selecting the value of $X_{\rm rcn}$.

In an IPT system, $\eta_{\rm link}$ is maximised for a given value of $R_{\rm ac}$, as shown in (5). Therefore, the RCN Class D rectifier can be designed to inherently present the optimal load to the IPT system for a broad range of dc-load values.

B. Load-Independent Class EF Inverter for Variable Coupling

The load-independent Class EF inverter was first proposed in [17]. It is a ZVS Class EF circuit that operates at a fixed duty cycle, achieves ZVS independent of the resistive load and inherently regulates the amplitude and the phase of the output current ($i_{\rm p}$) when the load changes. The solution for load-independent operation in the Class EF inverter [17] is similar to that found for a Class E inverter in [29]. The load independent Class EF inverter, however produces a constant amplitude output current as opposed to the constant amplitude output voltage achieved with the Class E. This characteristic makes the load-independent Class EF inverter more suitable to drive an IPT-coil, without requiring an impedance matching

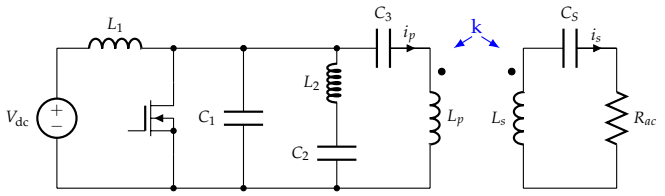


Fig. 6. Load-independent Class EF inverter in an IPT system.

network. Additionally, The load-independent Class EF inverter has a better power output capability, which is a general advantage of the EF topology against the Class E [30].

The Class EF topology, shown in Fig. 6 has been extensively analysed in [30]–[32] to characterise the circuit and develop the design equations for different tuning methods. A Class EF inverter is a hybrid between a Class E and a Class F inverter in which the additional LC network, comprised of C_2 and L_2, shapes the voltage and current through the transistor, and gives an additional two degrees of freedom in the circuit design. This topology has been widely utilised to reduce the peak voltage in the transistor by tuning C_2 and L_2 at the second or third harmonic of the switching frequency, hence by shaping the voltage across the transistor to reduce the peak values, higher throughput power can be achieved for a given device rating. Contrastingly, in the load-independent design, the additional branch is tuned between the first and second harmonic of the switching frequency. Load-independent operation is achieved by solving the state-space equations of the circuit, setting as a point of convergence that the voltage in the transistor is zero at turn-on, independent of the resistive load. Infinite mathematical solutions that comply with this condition can be found; however, not all of these solutions are practical. Practical solutions are usually found by optimising the duty cycle for maximum power output capability of the transistor [17], [30], [31]. For the practical solutions that comply with the load independent criteria, the output current magnitude and phase are also independent of the load value.

Fig. 7 shows the waveforms of a theoretical solution for load-independent operation with the Class EF inverter. The drain-to-source voltage waveform converges to zero at $\omega t = 2\pi$ independent of the load, which demonstrates ZVS for the entire load range. Additionally, the amplitude and phase of the output current of the inverter ($i_{\rm p}$ in Fig. 6) do not change with load resistance.

The amplitude of the output current of the load-independent Class EF inverter is proportional to the input voltage and inversely proportional to the reactance of C_1 (X_{C_1}). This allows high level control in the IPT system to be performed by changing the input voltage. Nonetheless, since the average drain-to-source voltage of the switching device is equal to the input voltage, by changing its value, the effective capacitance C_1 changes due to the voltage-dependent drain-to-source capacitance of field-effect transistors ($C_{\rm oss}$). Large variations in input voltage can thus cause the inverter to become detuned.

The inherent properties of the load-independent Class EF inverter can be utilised in dynamic multi-MHz IPT to achieve high efficiency independent of coupling factor, since the con-

This work is licensed under a Creative Commons Attribution 3.0 License. For more information, see http://creativecommons.org/licenses/by/3.0/.

This article has been accepted for publication in a future issue of this journal, but has not been fully edited. Content may change prior to final publication. Citation information: DOI 10.1109/TPEL.2017.2768244, IEEE Transactions on Power Electronics

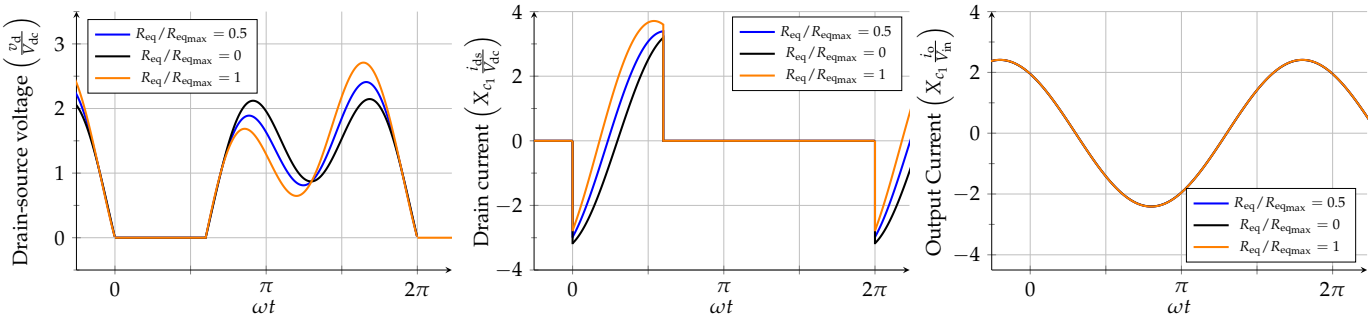


Fig. 7. Theoretical waveforms of the load-independent Class EF inverter.

verter maintains soft-switching independent of reflected load.

IV. Energy-Efficiency in Dynamic IPT Environments

In a dynamic IPT system where the amplitude of the current in the transmitting coil is constant and the ac-load resistance is fixed, the input power, the output power, and henceforth the dc-dc efficiency change over the range of motion of the dynamic environment with more power being transferred at higher coupling factors. It is fundamental to define an operating range for the coupling factor since it defines the range of reflected resistance seen by the transmitting-end and the range of induced electromotive force (EMF) in the receiving-end coil. The shape, position and alignment of the coils cannot be deduced from a value of k since it represents an infinite number of possible coil compositions. Hence, by designing the circuits to operate for a specified range of k, all geometrical compositions of the coils within this range (with an equal value of L and Q) are within the scope of the design. The design of the circuits can be done with the aim of achieving optimum efficiency for a particular value of k but also to have efficient operation for the entire range of k given Q and L.

In order to model the characteristics of a specific IPT-link and its dynamic nature, a probabilistic model will now be proposed, where the focus of design is set to achieve the maximum energy-efficiency over a predefined profile of k.

A. Energy-Efficiency for Variable Coupling Factor

The amount of energy that is delivered to the load for a given charging-time (t_0 to t_f) is defined, for a particular IPT system, as:

$$E_o\Big|_{t_0}^{t_f} = \int_{t_0}^{t_f} P_o\left(k, R_{ac}, i_{prms}\right) dt, \tag{13}$$

where P_o, in (6), is expressed as a function of variables k, R_{ac} and i_{prms}. The relative position and shape of the IPT-coils, and the surrounding materials determine the value of k. The inverter can be designed to achieve a constant value of i_{prms} or to increase i_{prms} as k decreases. In the latter case, in the formulation of (13), i_{prms} should be written as a function of k. Similarly, R_{ac} can be modified by having a power regulating circuit after the rectifier which would, for a series-tuned IPT system, decrease the value of R_{ac} when k decreases, in which case it should also be written as a function of k. The other parameters that define P_o are considered constants. It should be noted that (6) considers tuned circuits; hence, the input reactance of the rectifier is assumed to be zero at the frequency of operation.

A similar expression can be found for the total amount of energy extracted from the dc-source,

$$E_i\Big|_{t_0}^{t_f} = \int_{t_0}^{t_f} P_i\left(k, R_{ac}, i_{prms}\right) dt, \tag{14}$$

to calculate the energy-efficiency as:

$$\eta_{avg} = \frac{E_o}{E_i}. \tag{15}$$

The dc-dc energy-efficiency is therefore equivalent to the weighted-average dc-dc power-efficiency of the IPT system throughout the charging-time.

B. Modelling the Coupling Factor as a Probability Distribution

In dynamic environments, k changes with time as the relative position of the coils change. If the relative position and the misalignments are predictable for the entire charging-time, k can be described as a function of time, and the energy-efficiency can be calculated as previously described. This approach, however, does not consider mobile autonomy of dynamic wireless charging environments where it is often impossible to predict the exact position and misalignment of the IPT-coils, and therefore describe k as a function of time.

Consequently, it can be more convenient to account for the unpredictability of k by treating it as a stochastic variable. The dynamic behaviour of k can be modelled using a probability-mass-function or a probability-density-function. If the parameters that determine the distribution of k have a discrete nature (for example having a fixed number of possible coil-positions), the distribution of k could be described using a probability-mass-function; this function describes the probability of k being taken the specific values associated with the finite number of possible relative positions of the coils. Alternatively, if the range of motion is continuous, k should be described as a probability-density-function ($f(k)$). The range of k (k_{min} to k_{max}) is determined by the range of motion of system and the probability distribution of k is determined by the dynamic

This work is licensed under a Creative Commons Attribution 3.0 License. For more information, see http://creativecommons.org/licenses/by/3.0/.

This article has been accepted for publication in a future issue of this journal, but has not been fully edited. Content may change prior to final publication. Citation information: DOI 10.1109/TPEL.2017.2768244, IEEE Transactions on Power Electronics

nature of the IPT environment, i.e. how the value of k is distributed for the period of charging-time.

From (13) and assuming that $R_{\rm ac}$ and $i_{\rm p_{rms}}$ are functions of k (or constant), the output-energy can therefore be described as the product of time and the expected value of $P_{\rm o}$:

$$E_{\rm o}\Big|_{t_0}^{t_{\rm f}} = (t_{\rm f} - t_0) \int_{k_{\rm min}}^{k_{\rm max}} P_{\rm o}\left(k\right) f\left(k\right) {\rm d}k. \tag{16}$$

The input-energy can also be calculated using the same probability-density-function $f(k)$ as:

$$E_{\rm i}\Big|_{t_0}^{t_{\rm f}} = (t_{\rm f} - t_0) \int_{k_{\rm min}}^{k_{\rm max}} P_{\rm i}\left(k\right) f\left(k\right) {\rm d}k, \tag{17}$$

and the energy-efficiency can be therefore calculated as:

$$\eta_{\rm avg} = \frac{\displaystyle\int_{k_{\rm min}}^{k_{\rm max}} P_{\rm o}\left(k\right) f\left(k\right) {\rm d}k}{\displaystyle\int_{k_{\rm min}}^{k_{\rm max}} P_{\rm i}\left(k\right) f\left(k\right) {\rm d}k}. \tag{18}$$

A possible design approach for IPT using this model, is to achieve the highest energy-efficiency by finding the system design that reaches the maximum value of $\eta_{\rm avg}$ in (18). Considering that the optimisation of $\eta_{\rm avg}$ also depends on the design of the magnetics and the power throughput control, a practical guideline to design the circuits at both ends of the system, is to aim for the highest power efficiency at the value of k that reaches a maximum in the function $P_{\rm o}(k)f(k)$, which is the point of maximum energy throughput.

C. Describing an IPT-Link and its Dynamics with a Probability Density Function

The probability-density-function $f(k)$ represents the dynamics of an IPT system in a way that is useful for the circuit design and evaluation. It not only determines the range of k at which the circuits operate but also the determines which values of k have a higher impact on the energy-efficiency of the system. The function $f(k)$ can be obtained by determining the probability distribution of the relative position of the coils $g(x_1, ..., x_n)$ for the defined charging time as follows:

$$\int_{x_{1_{\rm min}}}^{x_{1_{\rm max}}} ... \int_{x_{\rm n_{min}}}^{x_{\rm n_{max}}} g(x_1, ..., x_n) {\rm d}x_1 ... {\rm d}x_n = 1, \tag{19}$$

where, $x_1, ..., x_n$ are the variables that determine the relative position of the coils (e.g. linear misalignment, distance, angular misalignment), and n represents the number of variables that affect the coupling factor. The function $g(x_1, ..., x_n)$ can be transformed to a probability-distribution of k by declaring k as a function of $x_1, ..., x_n$. Several mathematical models to characterise k as a function of distance and misalignments can be found in literature for different coil designs, for example [33] can be used for circular coils and [34] for planar coils. After analysing the dynamic behaviour of the system to determine the probability of the relative position and misalignment of the coils, a density-function transformation should be performed to obtain the function $f(k)$, which describes the probability distribution of k for the determined charging time.

TABLE I
COMPONENTS AND VALUES FOR THE DYNAMIC-IPT CIRCUITS DESIGN

Component	Value (6.78 MHz)	Value (13.56 MHz)	Description
$L_{\rm p}$ (nH)	980	989	
$R_{\rm p}$ (Ω)	0.053	0.054	
L_s (nH)	984	990	
R_s (Ω)	0.051	0.052	
C_1 (pF)	469+$C_{\rm oss}$	180+$C_{\rm oss}$	Vishay QUAD HIFREQ
C_2 (pF)	418	180	Vishay QUAD HIFREQ
C_3 (pF)	1003	190	Vishay QUAD HIFREQ
L_1 (μH)	88	88	Wurth Elektronik WE-PD
L_2 (nH)	404	270	Coilcraft 2014VS
$R_{\rm eq}$ (Ω)	up to 6.00	up to 5.00	reflected resistance
C_s (pF)	560	147	Vishay QUAD HIFREQ
$C_{\rm rcn}$ (nF)	7.06	3.11	Johanson Technology E
$L_{\rm rcn}$ (nH)	78	42	Coilcraft 2014VS
$R_{\rm dc}$ (Ω)	5 to 120	5 to 120	dc-load resistance
C_o (μF)	1	1	Murata GRM Series
Q_1	GS66504B (650 V, 15 A) GaN FET		
D	10 A, 120 V Schottky diodes (FSV10120V)		

V. CASE STUDY AND EXPERIMENTAL VERIFICATION

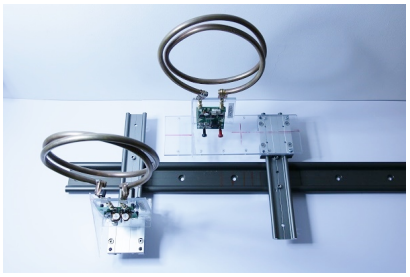
A case study was performed using the proposed inherently regulated resonant circuits. Namely, a load-independent Class EF inverter that achieves ZVS and feeds a constant amplitude current to the transmitting-end coil, and a RCN Class D rectifier with an input resistance designed to match the optimal ac-load for a broad range of dc-loads. The topologies of the rectifier and the inverter are shown in Fig. 4 and Fig. 6 respectively, and the designed values are shown in Table I.

The purpose of this case study is to evaluate the performance of the proposed IPT system in a dynamic charging environment by measuring the dc-dc efficiency, and how it changes against k and $R_{\rm dc}$. Changes in k represent changes in the relative position of the coils, and changes in $R_{\rm dc}$ represent changes in the input resistance of an additional power conversion stage, or a dc-load. The coupling factor was altered by changing the position of the receiving end coil as shown in Fig. 8, and measurements for a broad range of load resistance were performed at each coupling. Fig. 8 also shows the coils used in this experiment, which consist of a two-turn copper pipe conductor with an average diameter of $17.5\,{\rm cm}$. Photographs of the experimental layout and the circuit boards are shown in Fig. 9. The self-inductance and ESR values of the coils were measured using a Keysight E4990A Impedance Analyser and are shown in Table I.

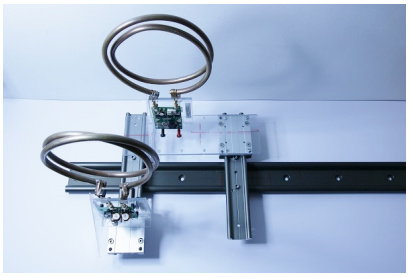
Two designs are presented: one for a frequency of operation of $6.78\,{\rm MHz}$ and another one for $13.56\,{\rm MHz}$. Both designs use the same IPT-coils, the same PCB layouts and the same switching devices but with different circuit tuning; however, in order to obtain a similar range in output power, the coil-separation was set at $11\,{\rm cm}$ for the experiment at $6.78\,{\rm MHz}$, and at $17.8\,{\rm cm}$ for the one at $13.56\,{\rm MHz}$. The objective of performing experiments at two different frequencies is to confirm the advantages and limitations of the topology and verify

This work is licensed under a Creative Commons Attribution 3.0 License. For more information, see http://creativecommons.org/licenses/by/3.0/.

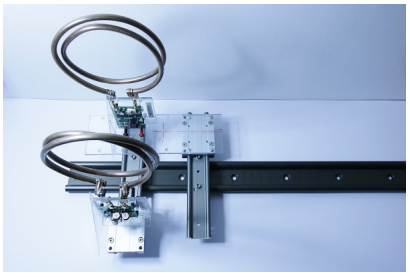
This article has been accepted for publication in a future issue of this journal, but has not been fully edited. Content may change prior to final publication. Citation information: DOI 10.1109/TPEL.2017.2768244, IEEE Transactions on Power Electronics



(a) coils with a separation of 17.8 cm and a misalignment of 18.3 cm.



(b) coils with a separation of 17.8 cm and a misalignment of 9.0 cm.



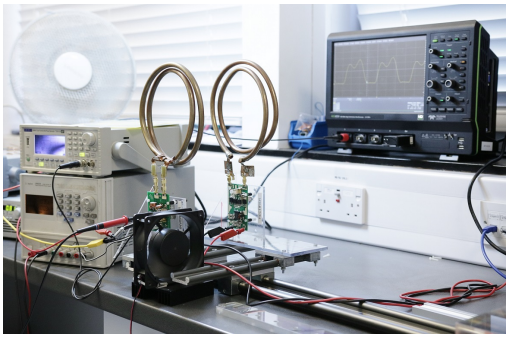
(c) perfectly aligned coils with a separation of 17.8 cm.

Fig. 8. Experimental set-up for variable coupling factor in an IPT system.

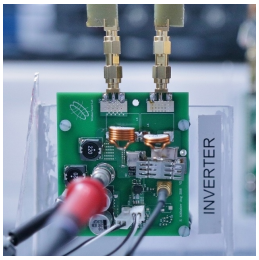
the performance against changes in k or R_{dc} while analysing the benefits and limitations of increasing the frequency of operation. Although the design objective is the same for both cases, there are subtle differences in the approach taken on each design. These differences are indicated and explained in the respective sections.

Measurements were taken for a sensible range of coil misalignments, dc-load values and dc-input voltages. The results of the experiments for variable R_{dc} are shown in Fig. 10 and the results for variable k are shown in Fig. 12.

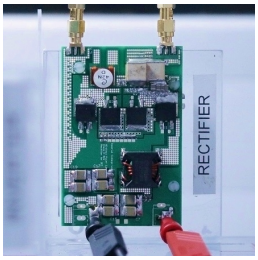
After describing the output power and the dc-dc efficiency in terms of k, the output-energy and the energy-efficiency were calculated using the proposed model, assuming a uniform distribution in the relative motion of the coils. This distribution represents a charging scenario in which the load moves at constant velocity over the charging pad, i.e. with a constant speed of motion on the x axis with constant values of y and z. The distribution of k was calculated using the function $k(x)$ shown in Fig. 13.



(a) photograph of the experimental layout.



(b) photograph of the inverter board.



(c) photograph of the rectifier board.

Fig. 9. Photographs of the experimental layout showing the transmitter and receiver side of the IPT system mounted on a linear slide, the oscilloscope, the signal generator and the gate-voltage power supply.

A. Design Considerations for Variable Coupling

In (6) and (7), the output power is defined as a function proportional to k^2 and R_{ac}^{-1}, therefore as these variables change, the output power is also prompted to change. For this case study both $i_{\mathrm{p_{rms}}}$ and R_{dc} were kept constant for every step in k, and $i_{\mathrm{p_{rms}}}$ and k were kept constant for every step in R_{dc}. Hence, considering that these variables were not adjusted to perform power regulation, the case study represents an uncontrolled load designed for maximum energy-efficiency. In order to achieve this, the design was performed for highest dc-dc efficiency at $k_{\max}$, since the energy throughput function $P_{\mathrm{o}}(k)f(k)$ reaches its maximum at $k_{\max}$ for the particular dynamic behaviour of this case study. It should be noted that if the output power was regulated (by controlling either i_{p} or R_{dc}) or the relative motion of the coils had a different distribution (e.g. a vehicle with exponentially decreasing velocity as the misalignment between the coils increases), the value of k that should be used to optimise the circuits, which corresponds to the value that achieves the maximum η_{avg} in (18), might differ from $k_{\max}$.

The variable that defines the highest output power capability of the system, and also influences the designs of the circuits at both ends of the IPT system is k, since it determines the values of $R_{\mathrm{ac_{opt}}}$ and R_{eq} (for a particular ac-load). Knowledge of the range of values of R_{eq} is necessary to design the inverter, and the value of $R_{\mathrm{ac_{opt}}}$ at maximum coupling is necessary to design the rectifier (for maximum link-efficiency at maximum coupling). Table II shows these variables for both designs, which were calculated using the measured range of k of the IPT configurations previously defined, and the component values presented in Table I.

This work is licensed under a Creative Commons Attribution 3.0 License. For more information, see http://creativecommons.org/licenses/by/3.0/.

This article has been accepted for publication in a future issue of this journal, but has not been fully edited. Content may change prior to final publication. Citation information: DOI 10.1109/TPEL.2017.2768244, IEEE Transactions on Power Electronics

TABLE II
SCOPE OF THE EXPERIMENTS

Case study	Wireless air-gap	k	$R_{\mathrm{ac_{opt}}}(k_{\max})$	$R_{\mathrm{eq}}(R_{\mathrm{ac_{opt}}})$
6.78 MHz	11 cm	0-10.5 %	4.92Ω	0- 5.06Ω
13.56 MHz	17.8 cm	0-4.5 %	3.91Ω	0- 4.24Ω

B. Design of the RCN-Class D Rectifier

The rectifier was designed to achieve the highest efficiency considering the distribution of values of k during the experiment. Schottky diodes with very low forward voltage were chosen, and high-Q passive components were chosen to complete the circuit. The values and description of the components for both designs are shown in Table I.

The parameter X_{rcn}, which corresponds to the reactance of each of the passive components of the RCN, was chosen to be slightly lower than $R_{\mathrm{ac_{opt}}}(k_{\max})$ in order to match the optimal ac-load with R_{dc} at a higher (or lower) value than $\frac{\pi^2}{4}X_{rcn}$ (the minimum value of R_{ac} is equal to X_{rcn}, and is theoretically reached at this point). It is worth noticing that according to (10) and the plots in Fig. 5, R_{ac} matches its optimal load at two values of R_{dc}, however the greater value of the two, achieves a higher efficiency given that the current in the diodes is lower at higher values of R_{dc}.

The design of the parameter X_{rcn} relative to the optimal ac-load is slightly different in both designs in order to show the advantages and limitations of designing this variable at two different values within the range $\left[0, R_{\mathrm{ac_{opt}}}\right]$. X_{rcn} is determined by selecting an inductor for the RCN in which the reactance, at the frequency of operation, meets the designed value for X_{rcn}. The design of the system at 13.56 MHz has an X_{rcn} equal to $0.91R_{\mathrm{ac_{opt}}}(k_{\max})$ and the one at 6.78 MHz has an X_{rcn} equal to $0.67R_{\mathrm{ac_{opt}}}(k_{\max})$. When the ratio of these two variables is closer to one, as can be seen in the plots for the design at 13.56 MHz in Fig. 10, the maximum efficiency point is closer to the maximum power peak, at which point the rectifier inherently regulates its input resistance, and therefore achieves power regulation against changes in R_{dc}. This effect can be best appreciated in Fig. 10a, since the design at 13.56 MHz has a higher X_{rcn}: for a variation in dc-load of 2.5-15 $R_{\mathrm{dc}}/X_{\mathrm{rcn}}$, corresponding to 100-17 % normalised load, a variation in output power of 44-56 W, corresponding to 100-78 %, was measured. Nonetheless, the dc-dc efficiency of the design at 6.78 MHz is remarkably high with a lower value of X_{rcn} and a higher R_{dc}. At maximum coupling, a dc-dc efficiency of 80-88 % was achieved with a power output ranging from 25-95 W. Since in this rectifier topology the RCN effectively amplifies the output current at lower dc-loads and maintains R_{ac} fairly constant, when the design of X_{rcn} with respect to $R_{\mathrm{ac_{opt}}}$ has a lower value, the losses in the rectifier decrease when R_{dc} is set to match $R_{\mathrm{ac_{opt}}}$, nonetheless a better compression is achieved when X_{rcn} is higher and $R_{\mathrm{ac_{opt}}}$ is reached with a lower value of R_{dc}.

C. Design of the Load-Independent Class EF Inverter

The inverter was designed as proposed in [17] with a duty cycle of 30 %, to achieve the highest power output capability of the transistor for this topology, and a tuning frequency of the additional LC branch of:

$$\frac{1}{2\pi\sqrt{L_2C_2}} = 1.67f_{i_{\mathrm{p}}}. \tag{20}$$

The following design equations were derived from the state space equations of the circuit by solving for $v_{\mathrm{d}} = 0$ at turn-on independent of R_{eq} and were utilised for both designs:

$$\begin{aligned} 2\pi f_{i_{\mathrm{p}}} R_{\mathrm{eq_{max}}} C_1 &= 0.118614, \\ \frac{C_1}{C_2} &= 1.329341, \\ \frac{i_{\mathrm{p_{rms}}} R_{\mathrm{eq_{max}}}}{V_{\mathrm{dc}}} &= 0.202496, \\ \frac{X_{\mathrm{res}}}{R_{\mathrm{eq_{max}}}} &= 0.342106, \end{aligned} \tag{21}$$

where X_{res} is residual reactance:

$$X_{\mathrm{res}} = 2\pi f_{i_{\mathrm{p}}} L_{\mathrm{p}} - \frac{1}{2\pi f_{i_{\mathrm{p}}} C_3}. \tag{22}$$

These design equations represent one of the infinite mathematical solutions for load independent operation with the Class EF topology, however not all the mathematical solutions are practical. The maximum ratings of all components have to be considered, and ideally C_1 should be significantly larger than C_{oss}, since C_{oss} changes drastically with voltage. These equations are meant to serve as a guideline and careful tuning with real components is necessary once the circuit is built.

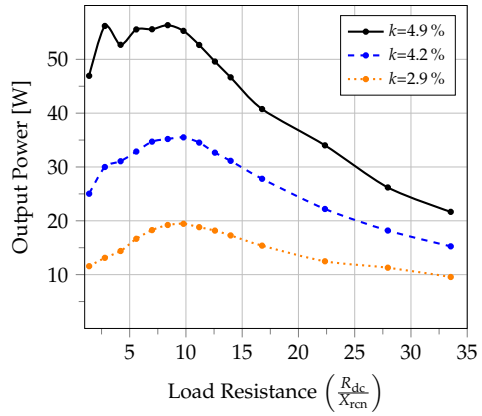
The load range was designed to be larger than $R_{\mathrm{eq_{max}}}$ (0-4 Ω), and the value of $i_{\mathrm{p_{rms-max}}}$, which is the maximum value of $i_{\mathrm{p_{rms}}}$ for a given design, was chosen to deliver a maximum of 150 W at full load. Fig. 11 shows the drain-to-source voltage from both experiments at maximum V_{dc} with an R_{eq} ranging from zero to maximum reflected resistance. The waveforms in Fig. 11 were plotted using data exported from a Teledyne LeCroy HDO4034 oscilloscope.

The inverter was built using a Gallium Nitride FET, and high-Q passive components to achieve the highest possible efficiency with commercially available components. The switching signal was provided by an external signal generator, which was connected to a high-speed power-FET driver by Intersil (ISL55110). The power consumption of the gate driver, measured at 86 mW at 6.78 MHz and 140 mW at 13.56 MHz, and the power consumption of an external fan (used as a precautionary measure), measured at 715 mW, are not included in the dc-dc efficiency calculations. The complete description of the components chosen for this design are shown in Table I.

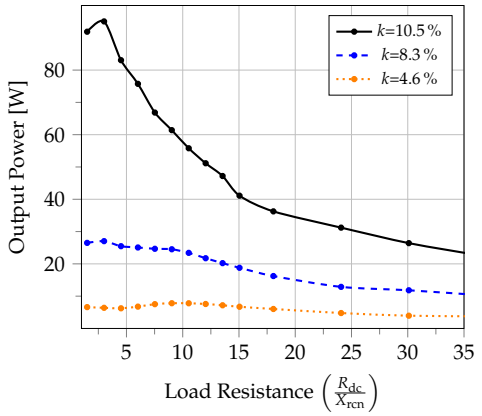
The losses in this topology were analysed in detail in [31]. For the proposed design, the losses in each of the LC branches, namely the one comprised of L_2 and C_2 and the other of L_{p} and C_3, can be deduced from the experimental waveforms shown in Fig. 11 and the ESR of the components. The losses in C_1 are included in the losses in the transistor. The losses in L_1 can be calculated considering its ESR and the dc-input current. The switching losses, according to [31], correspond

This work is licensed under a Creative Commons Attribution 3.0 License. For more information, see http://creativecommons.org/licenses/by/3.0/.

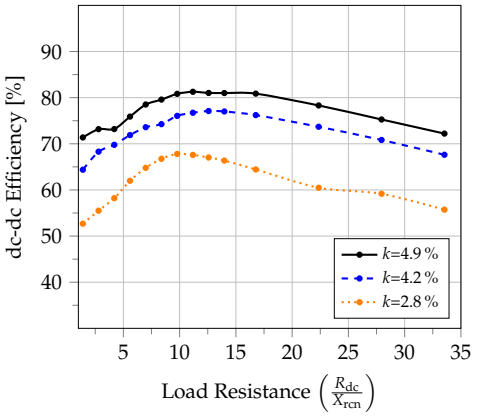
This article has been accepted for publication in a future issue of this journal, but has not been fully edited. Content may change prior to final publication. Citation information: DOI 10.1109/TPEL.2017.2768244, IEEE Transactions on Power Electronics



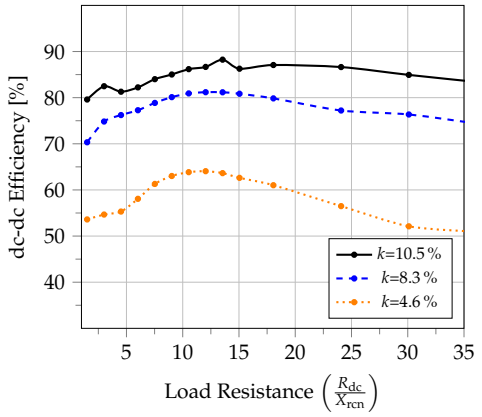
(a) Output power against R_{dc} at 13.56 MHz and a primary coil RMS current of $\frac{2}{3} i_{\mathrm{p_{rms-max}}}$.



(b) Output power against R_{dc} at 6.78 MHz and a primary coil RMS current of $\frac{3}{5} i_{\mathrm{p_{rms-max}}}$.

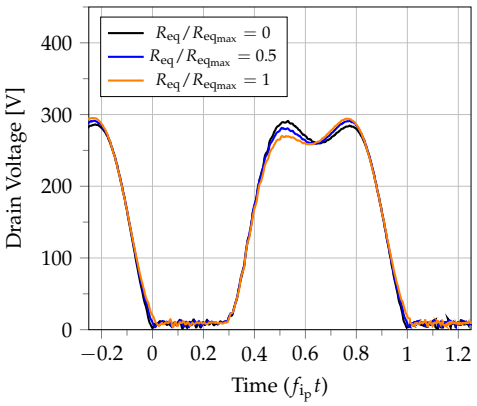


(c) dc-dc efficiency against R_{dc} at 13.56 MHz and a primary coil RMS current of $\frac{2}{3} i_{\mathrm{p_{rms-max}}}$.

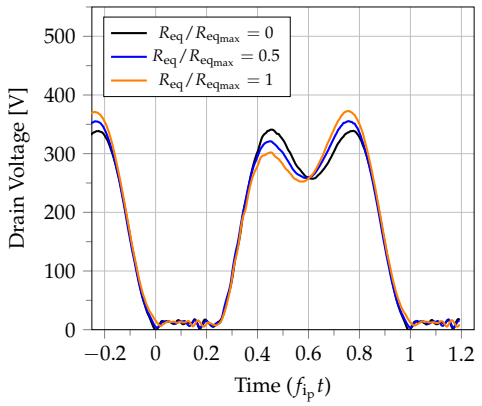


(d) dc-dc efficiency against R_{dc} at 6.78 MHz and a primary coil RMS current of $\frac{3}{5} i_{\mathrm{p_{rms-max}}}$.

Fig. 10. Experimental results for variable load resistance.



(a) Drain voltage waveform of the Class EF inverter at load independent operation. Plots taken from the experimental results for V_{dc}=150 V at 6.78 MHz.



(b) Drain voltage waveform of the Class EF inverter at load independent operation. Plots taken from the experimental results for V_{dc}=180 V at 13.56 MHz.

Fig. 11. Experimental results for variable coupling.

to $(\pi/6)\, f_{\mathrm{i_p}} t_{\mathrm{f}}$, where t_{f} is the fall time of the switch. The conduction losses depend on the $R_{\mathrm{ds_{on}}}$ of the transistor, which has a significant dependence of temperature [35]. Considering that measuring current at the different branches in multi-MHz converters is difficult due to the effects introduced by current probes, the distribution of losses here presented is based on a SPICE simulation, accounting for measured ESR values in all the inductances of the circuit: $P_{\mathrm{R_{eq}}}$ = 165.8 W, $P_{\mathrm{L_p - C_3}}$ = 2.2 W, $P_{\mathrm{L_2 - C_2}}$ = 2.7 W, $P_{\mathrm{L_1}}$ = 1.3 W, P_{FET} = 1.3 W for a calculated efficiency of 95.7 % in the inverter at

This work is licensed under a Creative Commons Attribution 3.0 License. For more information, see http://creativecommons.org/licenses/by/3.0/.

This article has been accepted for publication in a future issue of this journal, but has not been fully edited. Content may change prior to final publication. Citation information: DOI 10.1109/TPEL.2017.2768244, IEEE Transactions on Power Electronics

6.78 MHz. Similarly, at 13.56 MHz the efficiency is calculated at 95.1 % with the losses distributed as follows: $P_{\mathrm{R_{eq}}}$ = 153.2 W, $P_{\mathrm{L_p-C_3}}$ = 2.1 W, $P_{\mathrm{L_2-C_2}}$ = 2.5 W, $P_{\mathrm{L_1}}$ = 0.8 W, P_{FET} = 2.4 W.

D. Efficiency Measurements at Variable Coupling

Seven coil positions were chosen to characterise the output power and dc-dc efficiency against changes in the coupling factor. Fig. 12 shows the experimental results when performing a sweep in k.

It is shown that although the efficiency does deteriorate as k decreases, the rate of change is significantly compressed due to the properties of the chosen circuit topologies. For example, in the experiment at 6.78 MHz, when $i_{\mathrm{p_{rms}}}$ was set at a 60 % of its maximum value, the efficiency ranged from 88-70 % for a change in coupling of 2:1. That is a 20 % drop in efficiency for a 50 % drop in coupling.

The compressed dependence between efficiency and coupling is seen at all $i_{\mathrm{p_{rms}}}$ values in both designs. This is expected, because the link-efficiency is independent of $i_{\mathrm{p_{rms}}}$. Adjusting $i_{\mathrm{p_{rms}}}$ can however change the efficiency of the circuits which leads to changes in the dc-dc efficiency.

The inverter at 6.78 MHz was slightly detuned when large changes in the input voltage were performed. The input voltage variance of this design was not only larger than the 13.56 MHz version (40 % against 33 %) but also the range of values was set at lower voltage (90-150 V against 120-180 V). These changes had an effect on the parameter C_1 since the output capacitance of the GaN FET and its variance is much higher from 90 to 150 V than from 120 to 180 V [35]. At 6.78 MHz however, the values of the passive components are higher and therefore less vulnerable to parasitic capacitances and inductances, which allows a broader range of V_{dc} to be utilised in the design.

Considering that the effect of changing $i_{\mathrm{p_{rms}}}$, by adjusting V_{dc}, on the efficiency is low, it should be noted that V_{dc} can be used as a variable to perform power throughput control in this type of IPT systems.

E. Model of the Dynamic Environment

In order to calculate the output-energy and the energy-efficiency of the proposed case study, in which the load travels at constant velocity over a charging pad, a probability-density-function $g(x)$ describes the relative motion of the coils throughout the range of motion of the system ($x_{\min}$ to $x_{\max}$):

$$\int_{\mathrm{x_{min}}}^{\mathrm{x_{max}}} g(x)\mathrm{d}x = 1. \tag{23}$$

The constant velocity (v) from $x_{\min}$ to $x_{\max}$ in the time interval t_{f} to t_0 is then,

$$v = \frac{\partial x}{\partial t} = \frac{x_{\max} - x_{\min}}{t_{\mathrm{f}} - t_0}, \tag{24}$$

and the relative position should be represented as a uniform distribution:

$$g(x) = \begin{cases} \frac{1}{(x_{\max}-x_{\min})}, & x_{\min} \le x \le x_{\max} \\ 0, & x_{\min} > x > x_{\max}. \end{cases} \tag{25}$$

A variable transformation $k(x)$ should then be performed to model the probability-distribution of k, as opposed to the probability distribution of x, therefore (23) can be rewritten as:

$$\int_{k_{\min}}^{k_{\max}} -g\left(k\left(x\right)\right)\frac{\mathrm{d}x}{\mathrm{d}k}\mathrm{d}k = 1, \tag{26}$$

where $k_{\min}$ corresponds to $k(x_{\max})$ and $k_{\max}$ to $k(x_{\min})$. The probability-density-function of k is then defined as:

$$f(k) = -g\left(k\left(x\right)\right)\frac{\mathrm{d}x}{\mathrm{d}k}. \tag{27}$$

The function $k(x)$ was found experimentally and then fitted as a first order Gaussian function:

$$k(x) = k_{\max}\mathrm{e}^{-\frac{(x-\mathrm{b})^2}{\mathrm{c}^2}}, \tag{28}$$

where b represents the centre of the position of the peak (expected to be zero in this case study), and c represents the standard deviation ($\mathrm{c}^2 = 2\sigma^2$).

The function $x(k)$ is then calculated considering the mathematical restrictions for the variables and constants ($0 < k < k_{\max}, c \neq 0, x_{\min} < x < x_{\max}$):

$$x(k) = \mathrm{b} + \mathrm{c}\sqrt{\ln\left(\frac{k_{\max}}{k}\right)}, \tag{29}$$

then by deriving $x(k)$ with respect to k and substituting it in (27), the probability-density-function of k is represented as:

$$f(k) = \left(\frac{1}{x_{\max} - x_{\min}}\right)\frac{\mathrm{c}}{2k\sqrt{\ln\left(\frac{k_{\max}}{k}\right)}}. \tag{30}$$

Therefore, the output-energy for this particular case study can be calculated as:

$$E_{\mathrm{o}} = \frac{c}{2v}\int_{k_{\min}}^{k_{\max}} \frac{P_{\mathrm{o}}\left(k\right)}{k\sqrt{\ln\left(\frac{k_{\max}}{k}\right)}}\mathrm{d}k, \tag{31}$$

and the energy-efficiency as:

$$\eta_{\mathrm{avg}} = \frac{\displaystyle\int_{k_{\min}}^{k_{\max}} \frac{P_{\mathrm{o}}\left(k\right)}{k\sqrt{\ln\left(\frac{k_{\max}}{k}\right)}}\mathrm{d}k}{\displaystyle\int_{k_{\min}}^{k_{\max}} \frac{P_{\mathrm{i}}\left(k\right)}{k\sqrt{\ln\left(\frac{k_{\max}}{k}\right)}}\mathrm{d}k}. \tag{32}$$

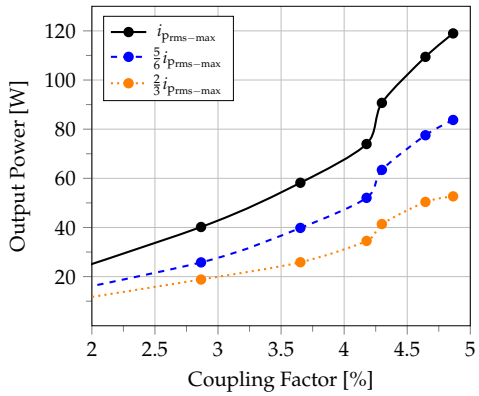
It should be noted that the proposed model does not depend on the way P_{o} is regulated against k. For example, if the power output is regulated to be constant (by controlling $i_{\mathrm{p_{rms}}}$ or R_{ac}), the input power would still change with k as previously defined, and therefore energy-efficiency can be calculated as:

$$\eta_{\mathrm{avg}}\Big|_{P_{\mathrm{o-constant}}} = \frac{(t_{\mathrm{f}} - t_0)P_{\mathrm{o}}}{\frac{c}{2v}\displaystyle\int_{k_{\min}}^{k_{\max}} \frac{P_{\mathrm{i}}\left(k\right)}{k\sqrt{\ln\left(\frac{k_{\max}}{k}\right)}}\mathrm{d}k}. \tag{33}$$

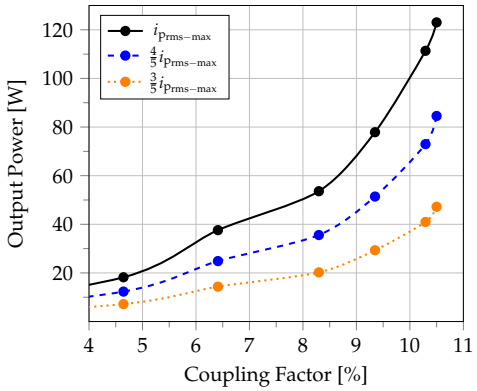
The distribution of k for both designs is shown in Fig. 13. This plot shows $k(x)$ from experimental verification and the fitted curve described by the Gaussian functions using the values from Table III. The experimental verification of k was achieved using a Keysight E4990A Impedance Analyser.

This work is licensed under a Creative Commons Attribution 3.0 License. For more information, see http://creativecommons.org/licenses/by/3.0/.

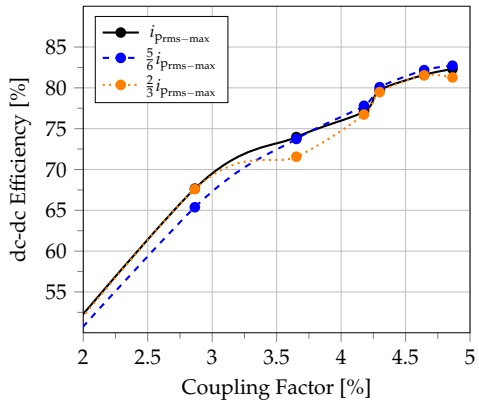
This article has been accepted for publication in a future issue of this journal, but has not been fully edited. Content may change prior to final publication. Citation information: DOI 10.1109/TPEL.2017.2768244, IEEE Transactions on Power Electronics



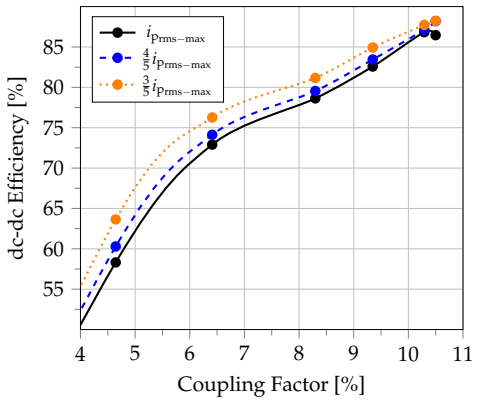
(a) Output power against k at 13.56 MHz and a dc-load resistance of 40 Ω.



(b) Output power against k at 6.78 MHz and a dc-load resistance of 45 Ω.

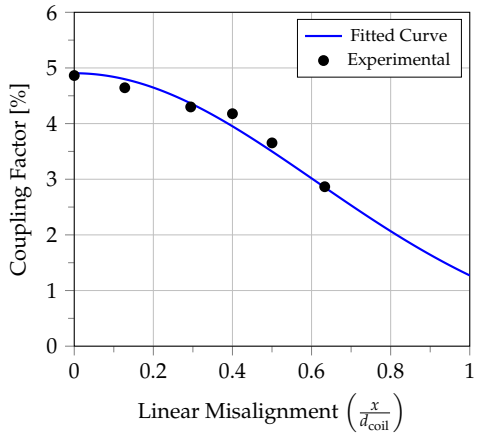


(c) dc-dc efficiency against k at 13.56 MHz and a dc-load resistance of 40 Ω.

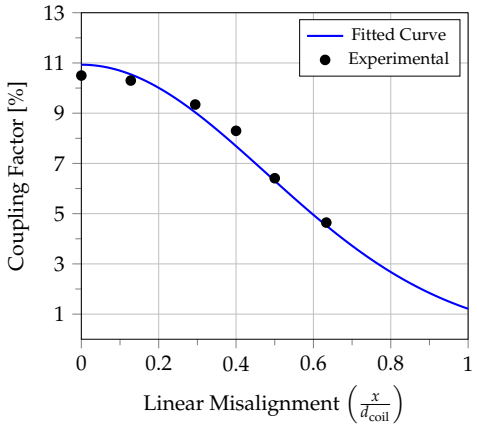


(d) dc-dc efficiency against k at 6.78 MHz and a dc-load resistance of 45 Ω.

Fig. 12. Experimental results for variable coupling.



(a) Coil separation of 17.8 cm.



(b) Coil separation of 11 cm.

Fig. 13. Coupling Factor against linear misalignment (normalised to a coil diameter distance) for a coil separation or 11 cm and 17.8 cm.

F. Energy-Efficiency Calculations

The output-energy and the energy-efficiency were calculated using (31) and (32), where P_{o} and P_{i} are defined as functions of coupling.

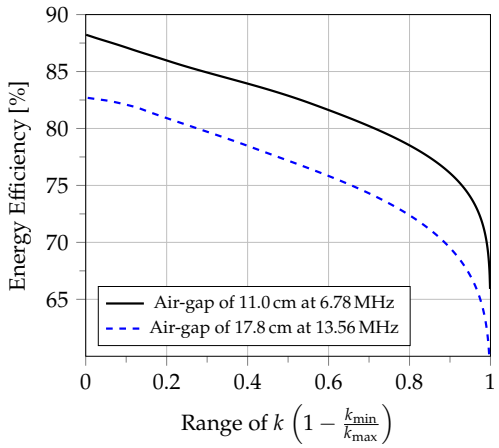
In order to evaluate how the relative motion of the coils affects the system's efficiency and energy throughput, both the energy-efficiency and the output-energy were calculated against the variable range of k, $k_{\min}$ to $k_{\max}$, as shown in Fig. 14. The range of k is determined by varying $k_{\min}$ from zero to $k_{\max}$, and the value of $k_{\max}$ is set as the coupling at zero misalignment. Moreover, in this case study, the value of $k_{\min}$ defines the tolerance to linear misalignment and the plots in Fig. 14 show the energy transferred to the load and the energy-efficiency against this variable.

This work is licensed under a Creative Commons Attribution 3.0 License. For more information, see http://creativecommons.org/licenses/by/3.0/.

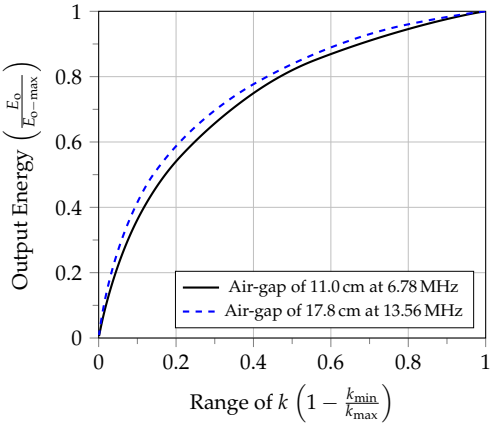
This article has been accepted for publication in a future issue of this journal, but has not been fully edited. Content may change prior to final publication. Citation information: DOI 10.1109/TPEL.2017.2768244, IEEE Transactions on Power Electronics

TABLE III
CONSTANTS VALUES FOR THE PROBABILITY DENSITY FUNCTION

Data from	Case study at	$k_{\max}$	b	c
Measurements	$6.78\,\mathrm{MHz}$	0.1093	-1.84×10^{-12}	0.1214
Measurements	$13.56\,\mathrm{MHz}$	0.0491	-4.184×10^{-13}	0.1549



(a) Calculated energy-efficiency against the range of motion of the system for the IPT system proposed in the case study.



(b) Calculated output-energy (normalised to the case with the highest k tolerance) against the range of motion of the system for the IPT system proposed in the case study.

Fig. 14. Calculation of output-energy and energy-efficiency.

There are certain advantages in analysing the output-energy and the energy-efficiency in terms of a variable range of k. Primarily, in a particular design, the range of motion (or the tolerance to misalignments $k_{\min}$) can be optimised to deliver a certain amount of energy to the load with a given limit set for energy-efficiency, considering that the energy-efficiency decreases against the range of k and the amount of energy increases with the range of k.

The analysis of the energy-efficiency against tolerance to changes in k can also be used to assess and improve the design of the IPT system and compare it against other designs. It is shown how in both systems in this case study, the energy-efficiency and output-energy have a very similar behaviour against variable range of k, which is expected considering that similar design approaches were used for both systems. The efficiency of the experiment at $6.78\,\mathrm{MHz}$ is better, but the values of k for this design are higher (the wireless air-gap is smaller). The losses at $13.56\,\mathrm{MHz}$ are higher mostly due to the switching losses in the semiconductor devices at higher frequencies. With the proposed circuit design, at $6.78\,\mathrm{MHz}$, an $80\,\%$ energy-efficiency is achieved for a tolerance to misalignments of $k_{\min} = 0.3k_{\max}$, and at $13.56\,\mathrm{MHz}$, a $74\,\%$ energy-efficiency is achieved for $k_{\min} = 0.3k_{\max}$. In both cases the energy-efficiency at this point is $90\,\%$ of the maximum power efficiency. It should be noted that the tolerance to misalignments of $0.3k_{\max}$ at $6.78\,\mathrm{MHz}$ represents a misalignment of $12.5\,\mathrm{cm}$ and at $13.56\,\mathrm{MHz}$ a misalignment of $17.25\,\mathrm{cm}$. This demonstrates the increased freedom of motion (larger wireless air-gaps and tolerance to misalignments) at higher frequencies with a trade-off in end-to-end efficiency.

VI. CONCLUSION

A combination of circuits that use inherent regulation properties of resonant converters was introduced and designed to achieve efficient operation independent of the coupling factor, in an IPT system working at multi-MHz frequencies. The result of the combination of the load-independent Class EF inverter and the RCN Class D rectifier is that high end-to-end efficiency is achieved across a broad range of coupling factors and dc-load values, representing a wide range of scenarios typical of dynamic wireless charging. Experiments were performed at $6.78\,\mathrm{MHz}$ and $13.56\,\mathrm{MHz}$ to demonstrate an IPT system capable of achieving high efficiency (up to $88\,\%$) with a significantly compressed dependence on k and R_{dc}.

A probability based model was introduced to analyse the energy-efficiency and the output-energy in terms of the range of motion of the dynamic charging system. The basis of the model is the function $f(k)$, a probability-density-function that models the distribution of k throughout the range of motion of the system for a given charging time, which represents the motion behaviour of the device being charged. The main advantages of calculating the output-energy and the energy-efficiency using this model is that primarily, for a particular design, the selection of the range of motion can be determined by considering the throughput energy and the energy-efficiency associated to the charging process. Also, by analysing the system as proposed, further optimisation, considering the mobility of the device being charged, can be achieved by tuning the circuits to a more accurate value of k which would improve the energy-efficiency, or by improving the design of the IPT-link to obtain a probability-density-function associated to a higher energy-efficiency or a broader range of motion.

ACKNOWLEDGMENT

The authors would like to acknowledge the following funding sources: the Department of Electrical and Electronic Engineering of Imperial College London, PINN Programme by the Ministry of Science and ICT of Costa Rica MICITT,

This work is licensed under a Creative Commons Attribution 3.0 License. For more information, see http://creativecommons.org/licenses/by/3.0/.

This article has been accepted for publication in a future issue of this journal, but has not been fully edited. Content may change prior to final publication. Citation information: DOI 10.1109/TPEL.2017.2768244, IEEE Transactions on Power Electronics

University of Costa Rica, EPSRC/EDF Case award number: 1401488, EPSRC Underpinning Power Electronics 2012: Components Theme; grant ref: EP/K034804/1 and EPSRC Underpinning Power Electronics 2012: Converters Theme; grant ref: EP/K035096/1.

REFERENCES

[1] G. Covic, J. T. Boys *et al.*, "Modern trends in inductive power transfer for transportation applications," *IEEE Trans. Emerg. Sel. Topics Power Electron.*, vol. 1, no. 1, pp. 28–41, 2013.

[2] R. Bosshard, J. W. Kolar, J. Mhlethaler, I. Stevanovi, B. Wunsch, and F. Canales, "Modeling and η - α -pareto optimization of inductive power transfer coils for electric vehicles," *IEEE Trans. Emerg. Sel. Topics Power Electron.*, vol. 3, no. 1, pp. 50–64, March 2015.

[3] S. Y. R. Hui, W. Zhong, and C. K. Lee, "A critical review of recent progress in mid-range wireless power transfer," *IEEE Trans. Power Electron.*, vol. 29, no. 9, pp. 4500–4511, Sept 2014.

[4] A. Zaheer, M. Neath, H. Z. Z. Beh, and G. A. Covic, "A dynamic EV charging system for slow moving traffic applications," *IEEE Trans. Transport. Electrific.*, vol. PP, no. 99, pp. 1–1, 2016.

[5] S. Li and C. C. Mi, "Wireless power transfer for electric vehicle applications," *IEEE Trans. Emerg. Sel. Topics Power Electron.*, vol. 3, no. 1, pp. 4–17, March 2015.

[6] A. Pacini, A. Costanzo, S. Aldhaher, and P. D. Mitcheson, "Design of a position-independent end-to-end inductive WPT link for industrial dynamic systems," in *IEEE MTT-S International Microwave Symposium (IMS)*, June 2017, pp. 1–3.

[7] S. Aldhaher, P. D. Mitcheson, J. M. Arteaga, G. Kkelis, and D. C. Yates, "Light-weight wireless power transfer for mid-air charging of drones," in *11th European Conf. on Antennas and Propagation (EUCAP)*, March 2017, pp. 1–5.

[8] M. Pinuela, D. C. Yates, S. Lucyszyn, and P. D. Mitcheson, "Maximizing dc-to-load efficiency for inductive power transfer," *IEEE Trans. Power Electron.*, vol. 28, no. 5, pp. 2437–2447, May 2013.

[9] G. Kkelis, J. Lawson, D. C. Yates, M. Pinuela, and P. D. Mitcheson, "Integration of a class-E low dv/dt rectifier in a wireless power transfer system," in *IEEE Wireless Power Transfer Conf. (WPTC)*, May 2014, pp. 72–75.

[10] S. Aldhaher, G. Kkelis, D. C. Yates, and P. D. Mitcheson, "Class EF_2 inverters for wireless power transfer applications," in *IEEE Wireless Power Transfer Conf. (WPTC)*, May 2015, pp. 1–4.

[11] J. M. Arteaga, S. Aldhaher, G. Kkelis, D. C. Yates, and P. D. Mitcheson, "Design of a 13.56 MHz IPT system optimised for dynamic wireless charging environments," in *2nd IEEE Annual Southern Power Electron. Conf. (SPEC)*, Dec 2016, pp. 1–6.

[12] M. Fu, H. Yin, M. Liu, and C. Ma, "Loading and power control for a high-efficiency class E PA-driven megahertz WPT system," *IEEE Trans. on Ind. Electron.*, vol. 63, no. 11, pp. 6867–6876, Nov 2016.

[13] J. Choi, D. Tsukiyama, Y. Tsuruda, and J. Rivas, "13.56 MHz 1.3 kW resonant converter with GaN FET for wireless power transfer," in *IEEE Wireless Power Transfer Conf. (WPTC)*, May 2015, pp. 1–4.

[14] S. Park and J. R. Davila, "Design of a class-DE rectifier with shunt inductance and nonlinear capacitance for high voltage conversion," *IEEE Trans. Power Electron.*, vol. PP, no. 99, pp. 1–1, 2017.

[15] D. C. Yates, S. Aldhaher, and P. D. Mitcheson, "Design of 3 MHz dc/ac inverter with resonant gate drive for a 3.3 kW EV WPT system," in *2nd IEEE Annual Southern Power Electron. Conf. (SPEC)*, Dec 2016, pp. 1–4.

[16] M. Liu, S. Liu, and C. Ma, "A high-efficiency/output power and low-noise megahertz wireless power transfer system over a wide range of mutual inductance," *IEEE Trans. Microw. Theory Techn.*, vol. PP, no. 99, pp. 1–9, 2017.

[17] S. Aldhaher, P. D. Mitcheson, and D. C. Yates, "Load-independent class EF inverters for inductive wireless power transfer," in *IEEE Wireless Power Transfer Conf. (WPTC)*, May 2016, pp. 1–4.

[18] K. Van Schuylenbergh and R. Puers, *Inductive powering: Basic theory and application to biomedical systems*. Springer Science & Business Media, 2009.

[19] C. H. Kwan, D. C. Yates, and P. D. Mitcheson, "Design objectives and power limitations of human implantable wireless power transfer systems," in *IEEE Wireless Power Transfer Conf. (WPTC)*, May 2016, pp. 1–4.

[20] S. Aldhaher, P. C. K. Luk, and J. F. Whidborne, "Tuning Class E inverters applied in inductive links using saturable reactors," *IEEE Trans. Power Electron.*, vol. 29, no. 6, pp. 2969–2978, June 2014.

[21] G. Kkelis, D. C. Yates, and P. D. Mitcheson, "Class-E half-wave zero dv/dt rectifiers for inductive power transfer," *IEEE Trans. Power Electron.*, vol. PP, no. 99, pp. 1–1, 2017.

[22] M. J. Schutten, R. L. Steigerwald, and M. H. Kheraluwala, "Characteristics of load resonant converters operated in a high power factor mode," in *Applied Power Electron. Conf. and Exposition. APEC '91*, Mar 1991, pp. 5–16.

[23] X. Xie, J. Zhang, C. Zhao, Z. Zhao, and Z. Qian, "Analysis and optimization of LLC resonant converter with a novel over-current protection circuit," *IEEE Trans. Power Electron.*, vol. 22, no. 2, pp. 435–443, March 2007.

[24] Y. Han, O. Leitermann, D. A. Jackson, J. M. Rivas, and D. J. Perreault, "Resistance compression networks for resonant power conversion," in *Power Electron. Specialists Conf. (PESC '05.)*, June 2005, pp. 1282–1292.

[25] ——, "Resistance compression networks for radio-frequency power conversion," *IEEE Trans. Power Electron.*, vol. 22, no. 1, pp. 41–53, Jan 2007.

[26] T. W. Barton, J. M. Gordonson, and D. J. Perreault, "Transmission line resistance compression networks and applications to wireless power transfer," *IEEE J. Emerg. Sel. Topics Power Electron.*, vol. 3, no. 1, pp. 252–260, March 2015.

[27] J. M. Arteaga, G. Kkelis, D. C. Yates, and P. D. Mitcheson, "A current driven Class D rectifier with a resistance compression network for 6.78MHz IPT systems," in *IEEE Wireless Power Transfer Conf. (WPTC)*, May 2016, pp. 1–4.

[28] M. K. Kazimierczuk and D. Czarkowski, *Resonant power converters*. John Wiley & Sons, 2012.

[29] R. E. Zulinski and K. J. Grady, "Load-independent class E power inverters. I. theoretical development," *IEEE Trans. Circuits Syst.*, vol. 37, no. 8, pp. 1010–1018, Aug 1990.

[30] Z. Kaczmarczyk, "High-efficiency Class E, EF_2 , and E/F_3 inverters," *IEEE Trans. on Ind. Electron.*, vol. 53, no. 5, pp. 1584–1593, Oct 2006.

[31] S. Aldhaher, D. C. Yates, and P. D. Mitcheson, "Modeling and analysis of Class EF and Class E/F inverters with series-tuned resonant networks," *IEEE Trans. Power Electron.*, vol. 31, no. 5, pp. 3415–3430, May 2016.

[32] ——, "Design and development of a Class EF_2 inverter and rectifier for multimegahertz wireless power transfer systems," *IEEE Trans. Power Electron.*, vol. 31, no. 12, pp. 8138–8150, Dec 2016.

[33] S. I. Babic and C. Akyel, "Calculating mutual inductance between circular coils with inclined axes in air," *IEEE Trans. Magn.*, vol. 44, no. 7, pp. 1743–1750, July 2008.

[34] Y. P. Su, X. Liu, and S. Y. R. Hui, "Mutual inductance calculation of movable planar coils on parallel surfaces," *IEEE Trans. Power Electron.*, vol. 24, no. 4, pp. 1115–1123, April 2009.

[35] *Bottom-side cooled 650 V E-mode GaN transistor, GS66504B datasheet*, GaN Systems, 2009, rev. 170321.

This work is licensed under a Creative Commons Attribution 3.0 License. For more information, see http://creativecommons.org/licenses/by/3.0/.